Transient Simulation of Distributed Networks Using Delay Extraction Based Numerical Convolution

Sourajeet Roy and Anestis Dounavis, *Member, IEEE*

***Abstract*—This paper presents a numerical convolution based approach for transient simulation of distributed networks characterized by band limited frequency domain data when terminated with arbitrary nonlinear circuits. The proposed algorithm uses time-frequency decompositions to extract multiple propagation delays of a distributed network and the associated attenuation losses in a piecewise manner, and implements inverse fast Fourier transform to efficiently convert the frequency response into a sum of delayed time domain responses. Numerical examples illustrate that the proposed algorithm shows significantly more accurate results for networks with multiple long delays when compared to existing numerical convolution techniques.**

***Index Terms*—Delay extraction, impulse response, numerical convolution, transient analysis, transmission lines.**

I. Introduction

DUE TO THE design complexity of high-frequency circuits, developing analytical interconnect models is a challenging task for the case when there are non-uniformities, process variations, and complex geometries. Under these circumstances, the behavior of interconnects lumped with other electromagnetic modules such as vias, connectors, and packages is often characterized by tabulated data, obtained by measurements or by electromagnetic simulations [1]–[25]. As a result, macromodeling techniques have become necessary to embed electromagnetic components characterized by tabulated data within a nonlinear circuit simulation environment. Typically, when dealing with long, low-loss interconnects, delay extraction of the line is required to provide accurate and efficient macromodels [8]–[15], [22]–[30].

Presently, two approaches exist for simulating delay extraction based macromodels of interconnect networks characterized by band limited frequency domain data. One approach is based on delayed rational functions [8]–[15]. These techniques extract the propagation delays from the tabulated data while the remaining attenuation losses of the frequency response are approximated using rational curve fitting [1]–[5]. This allows the time domain transfer function to be obtained as a sum of delayed exponentials which can be convoluted with any given input using the recursive convolution technique [31]. However, the memory and time complexities associated with approximating the attenuation losses using rational functions scale as $O(P^2N_p^2)$ and $O(P^4N_p^3)$, respectively, where P is the number of ports and N_p is the number of identified poles [23]. Hence, the curve fitting process for large multiport networks can be computationally intensive.

An alternative approach [23]–[25] seeks to first estimate the attenuation losses of the transfer function as tabulated data using a Hilbert transform [32]–[34] and use the result of the Hilbert transform to extract the dominant delay. Using inverse fast Fourier transform (IFFT) [35] and enforcing the extracted delay yields a delay-causal response, which is defined as an impulse response equal to zero for $t < t_p$, where t_p is the propagation delay of the system [23]. This approach explicitly enforces the finite delay for the excitation to travel from the input port to the output port. Hence, this provides more accurate transient results compared to directly implementing IFFT on the data. This is due to the fact that directly implementing IFFT on the data does not ensure a delay causal response, thereby resulting in inaccurate signal integrity quantities like eye diagram simulations as illustrated in [24] and [25]. The typical memory and time complexities to convert the multiport frequency domain data into the time domain impulse response using IFFT scale as $O(P^2N_t)$ and $O(P^2N_t \ln N_t)$, respectively, where N_t is the number of time points. These costs are very close to the optimal memory and time complexities of $O(P^2N_t)$ each, since the associated costs are independent of the number of poles/residues required for fitting the data using rational models [23]. However, for networks with multiple delays, extracting only one dominant delay may not yield reliable results since the attenuation loss function may possess non-negligible phase contributions due to the unextracted higher order delays and can no longer be considered as a pure minimum phase response. Thus, applying Hilbert transform to evaluate the attenuation losses for a general network with multiple unextracted delays can lead to transient simulation errors [32].

In this paper, a numerical convolution technique is presented based on extracting multiple propagation delays and evaluating the corresponding attenuation losses in a piecewise manner. The propagation delays of the system are determined using a 2-D time-frequency transform similar to [10]–[12]. Once the delays are determined, the attenuation losses associated

Manuscript received April 26, 2010; revised July 26, 2010; accepted September 28, 2010. Date of current version February 11, 2011. This work was supported by the Natural Sciences and Engineering Research Council of Canada, the Canada Foundation for Innovation, the Ontario Ministry of Research and Innovation-Early Research Award, and Canadian Microelectronics Corporation. This paper was recommended by Associate Editor L. M. Silveira.

The authors are with the Department of Electrical and Computer Engineering, University of Western Ontario, London, ON N6A 5B9, Canada (e-mail: sroy33@uwo.ca; adounavis@eng,uwo.ca).

Color versions of one or more of the figures in this paper are available online at http://ieeexplore.ieee.org.

Digital Object Identifier 10.1109/TCAD.2010.2090065

with the delays are obtained piecewise as pure data by appropriately partitioning the time-frequency plane. This approach differs from [10]–[12] which seek to collectively capture all the attenuation losses using a global iterative curve fitting technique. On determining the attenuation losses, enforcing the evaluated delays and implementing IFFT leads to an accurate representation of the transfer function in the time domain as a sum of delayed-causal responses. This yields more accurate transient results when compared to existing numerical convolution techniques such as direct implementation of IFFT on the data [18]–[21] or single delay extraction combined with IFFT [23]–[25]. This will be illustrated in the numerical examples of Section IV.

The organization of this paper is as follows. Section II discusses the theoretical background in detail and reviews the general class of time-frequency decompositions and Section III demonstrates the use of time-frequency decompositions to develop the proposed algorithm. Numerical examples and concluding remarks are provided in Sections IV and V, respectively.

II. Theoretical Background and Review of General Time-Frequency Decompositions

A. Theoretical Motivation

For ease of presentation, it is assumed that the tabulated data of any general multiport network is described in terms of the $\boldsymbol{Y}$-parameters similar to [8]–[15], as

$$\boldsymbol{Y}(s) = [Y_{ij}(s)] \qquad (i, j \in 1, .., P) \tag{1a}$$

$$Y_{ij}(s) = \sum_k Y_{ij}^{(k)}(s) e^{-sT_k} \tag{1b}$$

where T_k is the kth propagation delay, $Y_{ij}^{(k)}(s)$ is the attenuation losses corresponding to the kth propagation delay, "s" represents the Laplace variable, $[0{:}F_{\max}]$ is the bandwidth of interest, and P are the number of ports of the network. The time domain representations of $\boldsymbol{Y}$-parameters of (1) are

$$Y_{ij}(t) = \sum_k Y_{ij}^{(k)}(t - T_k) \tag{2}$$

where $Y_{ij}^{(k)}(t)$ is the inverse Fourier transform of $Y_{ij}^{(k)}(s)$.

Evaluating $Y_{ij}(t)$ using direct IFFT on the $Y_{ij}(s)$ without delay extraction results in errors in early time [18]–[21] leading to inaccurate signal integrity verification such as eye diagram simulations [24], [25]. One approach to reduce these errors is to extract the dominant propagation delay of the system [23]–[25], as

$$Y_{ij}(s) = H_{ij}(s) e^{-sT} \tag{3}$$

where T is the dominant propagation delay and $H_{ij}(s)$ correspond to the attenuation losses of the overall system. This approach produces accurate results when the system is characterized by a single dominant delay since $H_{ij}(s)$ is considered a minimum phase response and is extracted using a Hilbert transform of $Y_{ij}(s)$ as illustrated in [23]–[25]. For networks characterized by multiple delays, extraction of the dominant delay T allows $H_{ij}(s)$ to be expressed as

$$H_{ij}(s) = \sum_{k=1} Y_{ij}^{(k)}(s) e^{-s(T_k - T)}. \tag{4}$$

Provided the delays are closely spaced, the phase contribution of all $e^{-s(T_k - T)}$ is relatively small. As a result, $H_{ij}(s)$ can still be approximated as a minimum phase response and accurately evaluated by applying Hilbert transform on (3). However, this methodology of evaluating the attenuation losses may not yield accurate results for the case of a general distributed network with multiple delays which are not grouped close together. For a general distributed network characterized by multiple delays, $H_{ij}(s)$ can no longer be considered a minimum phase response due to the non-negligible phase contributions of the multiple delays $e^{-s(T_k - T)}$ [32]. Thus, application of the Hilbert transform may lead to inaccurate approximation of $H_{ij}(s)$ [32].

In order to address the above issues, a methodology to extract multiple delays for generalized distributed networks delays using the time-frequency techniques is proposed. The next section briefly reviews the general class of time-frequency decomposition techniques to better explain the proposed algorithm.

B. General Time-Frequency Decompositions

The time-frequency decompositions are a class of transformations from a 1-D function, say $Y_{ij}(s)$, to a 2-D function $F_{ij}(\omega, \tau)$ that measures the variance of the function with respect to both frequency (ω) and time (τ) variables. The time-frequency transform of $Y_{ij}(s)$ is defined as [36]–[38]

$$F_{ij}(\omega, \tau) = \int_{-\infty}^{\infty} Y_{ij}(\zeta)\, W(\zeta - \omega) e^{j\zeta\tau} d\zeta \tag{5}$$

where $F_{ij}(\omega, \tau)$ is the 2-D inverse Fourier transform function, ω and τ are the angular frequency and time variables, respectively, $W(\zeta - \omega)$ is a window centered at $\zeta = \omega$ of prescribed width L, and $s = j\zeta$ represents a simple transformation of variable. The integral of (5) provides a mechanism to filter sections of $Y_{ij}(\zeta)$ using an arbitrary window as it sweeps the frequency axis within the prescribed bandwidth of interest, and takes the inverse Fourier transform of each section individually. In this paper, $W(\zeta - \omega)$ represents a Gaussian window which corresponds to a Gabor transform and provides optimal support in both the time and frequency domains [36]–[38]. The window width (or the standard deviation) can be chosen using the methodologies of [39] and [40]. For the examples of this paper, the window sizes used are determined using the procedure of [40], where the window size is scaled linearly as it slides over the bandwidth [0: $F_{\max}$]. The energy of the function $F_{ij}(\omega, \tau)$ can be calculated as

$$\eta_{ij}(\tau) = \int_{-\infty}^{\infty} |F_{ij}(\omega, \tau)|^2 d\omega. \tag{6}$$

The $\eta_{ij}(\tau)$ of (6) is a 1-D function localizing the variation of energy of $F_{ij}(\omega, \tau)$ with time and provides a method to extract

propagation delays embedded in any frequency domain data as illustrated in [10]–[12]. The inverse of (5) exists [36]–[40] and can be expressed as

$$Y_{ij}(\zeta) = \frac{1}{2\pi} \int_{-\infty}^{\infty} \int_{-\infty}^{\infty} F_{ij}(\omega, \tau)\, W(\zeta - \omega) e^{-j\omega\tau} d\omega d\tau. \quad (7)$$

The reconstruction of $Y_{ij}(\zeta)$ can also be derived by separating the time-frequency plane of (ω, τ) into smaller regions Ω_m, and performing the integral of (7) over each region as

$$Y_{ij}(\zeta) = \sum_{m=1} \tilde{Y}_{ij}^{(m)}(\zeta)$$

$$\tilde{Y}_{ij}^{(m)}(\zeta) = \frac{1}{2\pi} \int_{\Omega_m} \int F_{ij}(\omega, \tau)\, W(\zeta - \omega) e^{-j\omega\tau} d\omega d\tau \quad (8)$$

$$\bigcup_{m=1} \Omega_m = \Re^2$$

where the summation of each integral of (8) over the suitable chosen Ω_m area leads to the piecewise re-construction of the original function $Y_{ij}(\zeta)$.

The time-frequency techniques of (5)–(8) provide a mechanism to extract the delays and the associated losses from the data for general multiple delay networks.

III. Development of Proposed Algorithm

The objective of this paper is to use the time-frequency decompositions to predetermine the delays T_k and the corresponding attenuation loss components $Y_{ij}^{(k)}(s)$ in order to evaluate the components of (1).

A. Estimating Delays T_k

To determine the propagation delays T_k, the transform of (5) is used to convert the tabulated data of $Y_{ij}(s)$ to the time-frequency domain representation of $F_{ij}(\omega, \tau)$ and to obtain the energy distribution of $\eta_{ij}(\tau)$ using (6). From the resultant energy distribution $\eta_{ij}(\tau)$, the delays will appear as sharp peaks with significant energy contributions. To illustrate how the delays are evaluated, consider the example of Fig. 1 where the physical layout of the interconnect is described in Fig. 2 and the details of this example is provided in Example 1 of Section IV. This example consists of a three-port (*P1-P2-P3*) subnetwork consisting of coupled interconnects and terminated with a nonlinear inverter. The three-port network is characterized by its tabulated data in terms of the $\boldsymbol{Y}$-parameters up to 3.5 GHz. Identification of the delays is determined by following the procedure described in [12], which evaluates the energy content of local peaks of $\eta_{ij}(\tau)$ as

$$\hat{\eta}_{ij}^{(k)} = \frac{1}{2\pi} \int_{\tau_{k-1}}^{\tau_k} \eta_{ij}(\tau) d\tau \quad (9)$$

where τ_{k-1} and τ_k are time points corresponding to local minimums of $\eta_{ij}(\tau)$ bounding the kth local maxima of $\eta_{ij}(\tau)$.

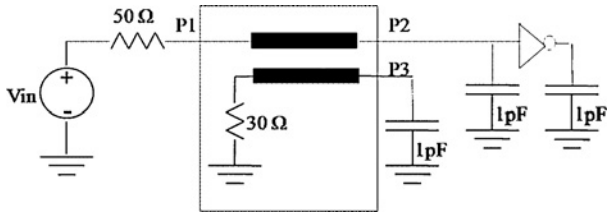

Fig. 1. Circuit layout of Example 1.

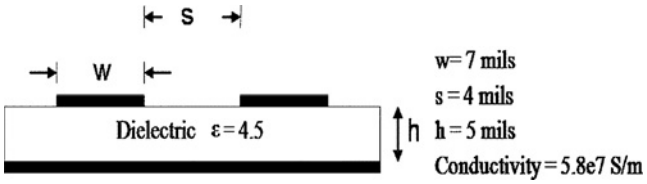

Fig. 2. Geometry of Example 1.

TABLE I
Delay Identification for Example 1 Using Time-Frequency Analysis

Identified Delays (ns)	Y_{11}	Y_{12}
T_1	2.25	1.27
T_2	2.54	3.42
T_3	4.49	3.81
T_4	4.79	5.66
T_5	5.08	6.05
T_6	–	6.35

All local maximums with relative energy contributions below a predefined tolerance ε are discarded.

$$\frac{\hat{\eta}_{ij}^{(k)}}{\sum_k \hat{\eta}_{ij}^{(k)}} < \varepsilon. \quad (10)$$

The value of ε is chosen such that the energy contribution of the neglected delays does not significantly affect the accuracy of the model and is problem dependent [12]. Fig. 3 illustrates the energy functions of $\eta_{11}(\tau)$ and $\eta_{12}(\tau)$ where the peaks of the function with significant energy contribution identified using (9), (10) and $\varepsilon = 1e-5$ are quantified in Table I

B. Partitioning the Time-Frequency Plane

In [10]–[12], the attenuation losses $Y_{ij}^{(k)}(s)$ of (1) are globally approximated as rational functions based on an iterative curve fitting technique. The objective of this paper is to avoid rational curve fitting due to the time and memory complexities involved [23] and express $Y_{ij}^{(k)}(s)$ as sampled data used in delayed numerical convolution. The proposed methodology seeks to represent the frequency contribution of a single or a group of delay peaks of $Y_{ij}(s)$ in terms of piecewise functions $\tilde{Y}_{ij}^{(m)}(s)$ using (8). In order to evaluate each $\tilde{Y}_{ij}^{(m)}(s)$, the Ω_m region of (8) needs to be determined. In this paper, the partitioning for of the (ω, τ) plane into Ω_m regions is determined by choosing the point t_k between two adjacent delays T_{k-1} and T_k where $\eta_{ij}(\tau = t_k)$ is the minima for $T_{k-1} < \tau < T_k$. If the value of

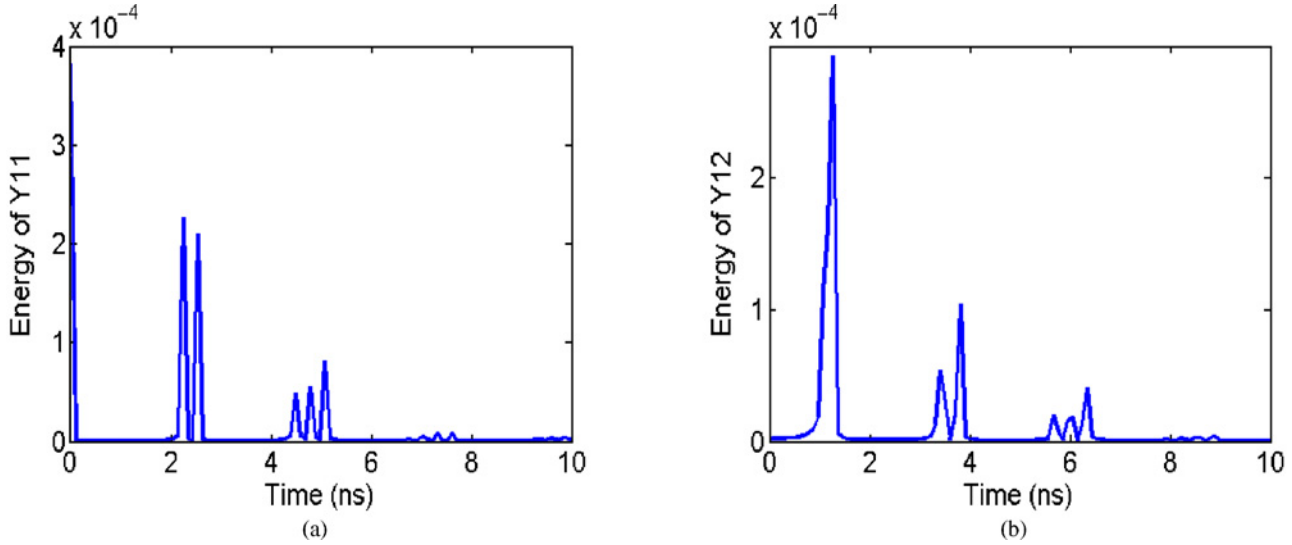

Fig. 3. Evaluating $\eta_{11}(\tau)$ and $\eta_{12}(\tau)$ of Example 1. (a) Energy of $|Y11|(\eta_{11}(\tau))$. (b) Energy of $|Y12|(\eta_{12}(\tau))$.

TABLE II
TIME AXIS PARTITIONING OF (ω, τ) PLANE OF EXAMPLE 1

Ω_m Regions	Y_{11}	Y_{12}
Ω_1	$0 \le \tau \le 1.00$ ns	$0 \le \tau \le 2.25$ ns
Ω_2	1.00 ns $\le \tau \le 3.00$ ns	2.25 ns $\le \tau \le 4.70$ ns
Ω_3	3.00 ns $\le \tau \le 6.00$ ns	4.70 ns $\le \tau \le 7.25$ ns

$\eta_{ij}(\tau = t_k)$ is below a certain predefined threshold δ

$$\eta_{ij}(\tau = t_k) < \delta \tag{11}$$

the point t_k is retained as a valid partitioning point, else it is discarded. The value of δ is chosen such that the valid partitioning point $(\tau = t_k)$ can effectively separate the energy contributions of two adjacent delays T_{k-1} and T_k from each other, thereby allowing a piecewise decomposition of $Y_{ij}(\zeta)$. Hence, δ depends on the energy distribution $(\eta_{ij}(\tau))$ of the given circuit and will vary for different circuit problems. Using (11) and the predefined threshold δ, the Ω_m regions are expressed as

$$\Omega_m \in \{(\omega, \tau) : 0 \le \omega \le 2\pi F_{\max}, t_k \le \tau \le t_{k+1}\}. \tag{12}$$

For the example of Fig. 1, the regions Ω_m, evaluated using (11)–(12) and $\delta = 1e-6$, are shown in Table II.

C. Estimating Attenuation Losses $Y_{ij}^{(k)}(s)$

Once the Ω_m regions are determined, the integral of (8) allows a piecewise reconstruction of the frequency domain data. For the case where there is only one identified delay peak in Ω_m, equating (1) with (8) yields

$$\tilde{Y}_{ij}^{(m)}(s) \approx Y_{ij}^{(m)}(s)e^{-sT_m} \tag{13}$$

where T_m is the extracted delay and $Y_{ij}^{(m)}(s)$ the associated attenuation losses within the region Ω_m. To evaluate the attenuation losses $Y_{ij}^{(m)}(s)$ from the band limited response of $\tilde{Y}_{ij}^{(m)}(s)$, the Hilbert transform is performed on (13) so as to ensure causality [32] as

$$\begin{aligned} |H_{ij}^{(k)}(s)| &= |\tilde{Y}_{ij}^{(k)}(s)| \\ \arg(H_{ij}^{(k)}(s)) &= -\frac{1}{2\pi}\rho \int_{-\pi}^{\pi} \ln|\tilde{Y}_{ij}^{(k)}(j\theta)| \cot\left(\frac{s - j\theta}{2j}\right) d\theta \end{aligned} \tag{14}$$

where ρ is the Cauchy's principal value. For the case when more than one identified delay exist in the region Ω_m, equating (1) with (8) yields

$$\tilde{Y}_{ij}^{(m)}(s) \approx \sum_{n=1}^{N} Y_{ij}^{(n,m)}(s)e^{-sT_{n,m}} \tag{15}$$

where N is the number of delays identified within Ω_m which are grouped together. In this case, the attenuation losses $Y_{ij}^{(n,m)}(s)$ may not be separately evaluated due to the energy spectrum of the delays $T_{n,m}$ overlapping each other. For this scenario (15) is approximated as

$$\begin{aligned} \tilde{Y}_{ij}^{(m)}(s) &= H_{ij}^{(m)}(s)e^{-sT_m} \\ H_{ij}^{(m)}(s) &= \sum_{n=1}^{N} Y_{ij}^{(n,m)}(s)e^{-s(T_{n,m}-T_m)} \end{aligned} \tag{16}$$

where T_m is the unknown dominant delay and $H_{ij}^{(m)}(s)$ is the corresponding unknown attenuation losses within the region Ω_m. Since the identified delay peaks in the region Ω_m lie close to each other (see Fig. 3), the phase contributions of each $e^{-s(T_{n,m}-T_m)}$ associated with $H_{ij}^{(m)}(s)$ are relatively small. As a result $H_{ij}^{(m)}(s)$ can still be approximated as a minimum phase response and be evaluated using Hilbert transform as in (14). Once $H_{ij}^{(m)}(s)$ is determined, T_m of (16) can be evaluated using a technique similar to that proposed in [23].

Once the attenuation losses of (13) and (16) are obtained in terms of data, a simple IFFT can be performed in a piecewise manner to obtain the time domain response as illustrated in (2). To handle networks terminated using nonlinear circuits in

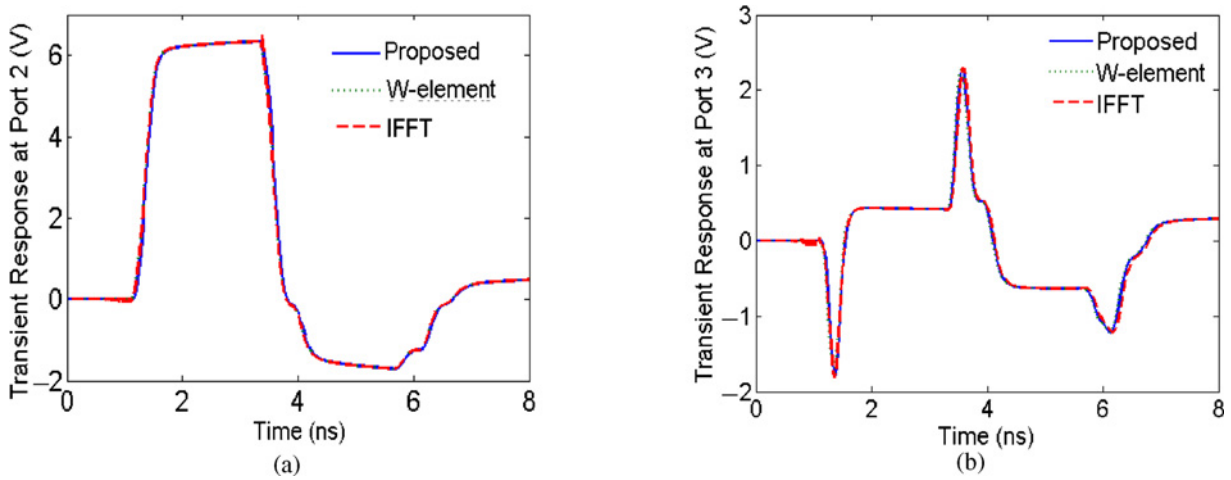

Fig. 4. Transient response of Example 1 using proposed algorithm, HSPICE's W-element, and direct IFFT. (a) Response of Port 2. (b) Response of Port 3.

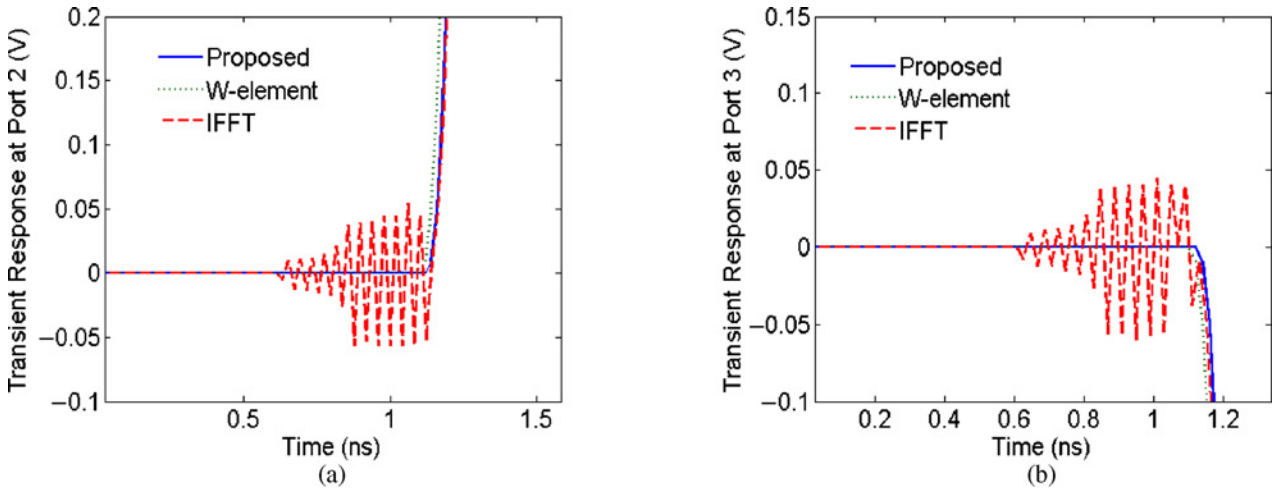

Fig. 5. Propagation delay capture of Example 1 using proposed algorithm HSPICE's W-element and direct IFFT. (a) Response of Port 2. (b) Response of Port 3.

a modified network analysis framework, the methodology of [23] is adopted.

The total computational cost to obtain the proposed model is mainly determined using (5) and (8). Equation (5) is equivalent to an IFFT operation which must be performed once for each terminal port response. The integral of (8) is similar to an FFT operation over each Ω_m partitions of each port response. Hence, this memory and time costs of (8) can be quantitatively expressed $O(P^2 N_t N_d)$ and $O(P^2 N_t N_d \ln N_t)$, respectively, where N_d is the average number of Ω_m partitions for each Y_{ij} defined as $N_d = (\sum_{i=1}^{P} \sum_{j=1}^{P} N_{ij})/P^2$, and N_{ij} is the number of Ω_m partitions for each Y_{ij}.

IV. Numerical Examples

Three examples are presented in this section to demonstrate the validity of the proposed algorithm. The results were obtained using MATLAB R2008a. In addition, since the examples selected had known structures, the transient responses obtained using proposed model were compared with HSPICE's W-element model [41], [42]. The bandwidths of interest of the examples are determined using the following rule of thumb $F_{\max} = 0.35/T_r$ as suggested in [43] and [44], where $F_{\max}$ is the maximum frequency of interest and T_r is the rise/fall time of the signal.

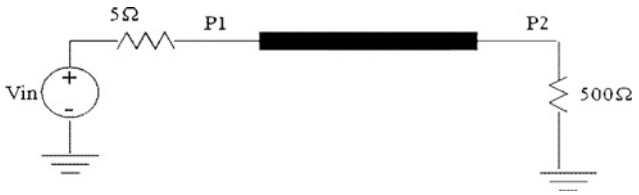

Fig. 6. Two-port circuit for Example 2.

Example 1: A three-port network is considered and shown in Fig. 1, where the physical layout of the interconnect is described in Fig. 2. The HSPICE field solver is used to obtain the p.u.l. parameters and includes the skin effect losses. The length of the transmission line is set to 20 cm.

The network is characterized by its terminal responses ($\boldsymbol{Y}$ parameters) over a bandwidth of 0–3.5 GHz. Using (5) and (6), the time-frequency transforms of $F_{ij}(\omega, \tau)$ and the energy

TABLE III
COMPARISON OF EXTRACTED DELAY USING TIME-FREQUENCY ANALYSIS WITH THEORETICAL VALUES FOR EXAMPLE 2

	Y_{11}			Y_{12}		
Value of "m"	Theoretical Delays $T_{11}^{(m)}$ (ns)	Observed Delays T_k (ns)	% Error	Theoretical Delays $T_{12}^{(m)}$ (ns)	Observed Delays T_k (ns)	% Error
0	0.00	0.00	0.00	8.00	8.00	0.00
1	16.00	15.98	0.13	24.00	24.02	0.08
2	32.00	31.07	0.22	40.00	39.96	0.10
3	48.00	47.95	0.10	–	–	–

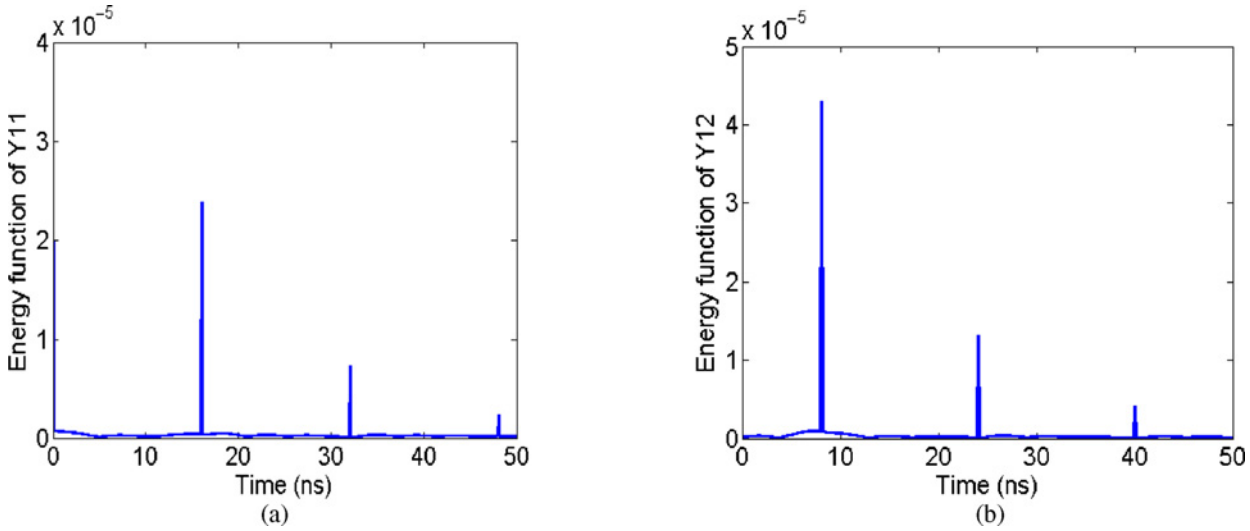

Fig. 7. Evaluating $\eta_{11}(\tau)$ and $\eta_{12}(\tau)$ of Example 2. (a) Energy of $|\mathrm{Y11}|(\eta_{11}(\tau))$. (b) Energy of $|\mathrm{Y12}|(\eta_{12}(\tau))$.

spectrums of $\eta_{ij}(\tau)$ for all the port-to-port Y-parameters are evaluated. The energy functions of $\eta_{11}(\tau)$ and $\eta_{12}(\tau)$ are shown in Fig. 3. Next, using (9) and (10) where $\varepsilon = 1e-5$, the delay peaks are identified as shown in Table I.

To obtain the attenuation loss responses in terms of sampled data, the (ω, τ) plane of $F_{ij}(\omega, \tau)$ is divided into Ω_m regions for the piecewise integral of (8). The partitioning of the time-frequency plane is implemented using (11) and (12), where $\delta = 1e-6$. The partitioning points for $Y_{11}(s)$ and $Y_{12}(s)$ are shown in Table II. Once $\tilde{Y}_{ij}^{(m)}(s)$ are evaluated using the integral of (8), the associated attenuation losses of (13) and (16) are obtained using the Hilbert transform on $\tilde{Y}_{ij}^{(m)}(s)$. Using the IFFT and enforcing the extracted delays, the terminal responses are described as a sum of delay-causal responses in the time domain. For a trapezoidal input pulse of rise time 0.1 ns and pulse width of 2 ns, the transient responses using the proposed algorithm are shown in Fig. 4. In addition, the proposed algorithm is compared with the transient results obtained by directly implementing IFFT on the tabulated data and HSPICE's W-element. It is observed that directly implementing IFFT on band limited data results in a transient response that is not delay-causal since the output voltage does not equal to zero for $t < t_p$ [23], where t_p is the propagation delay of the system as shown in Fig. 5. This may result in inaccurate signal integrity quantities, such as eye diagram simulations as reported in [24] and [25]. However, since the proposed algorithm and HSPICE's W-element model both use delay extraction to obtain the transient response, they provide similar responses.

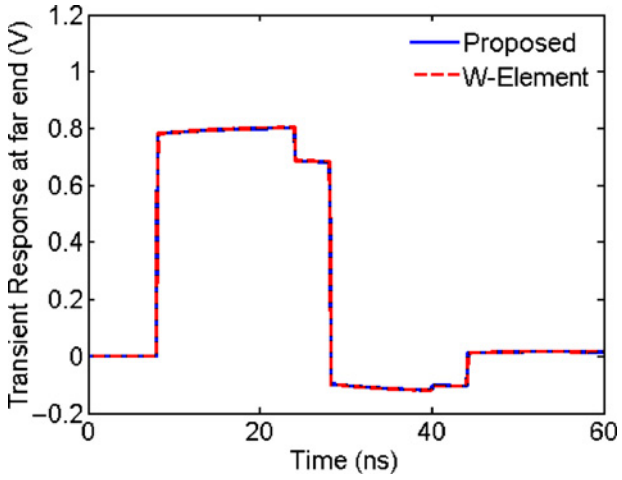

Fig. 8. Transient response at the far end of Example 2.

Example 2: In order to validate the accuracy of the delay extraction methodology proposed in Section III, a two-port example as reported in [9] (Fig. 6) is considered. The transmission line network has the resistive, inductive, and capacitive p.u.l. parameters of $R = 0.25\,\Omega/\mathrm{cm}$, $L = 4$ nH/cm, and $C = 1.6$ pF/cm, respectively, and a line length of $l = 100$ cm. Hence, the time-of-flight delay can be analytically determined as $T_0 = l\sqrt{LC}$. Due to mismatch of the termination impedance with the characteristic impedance of the line, the traveling TEM suffers multiple reflections at the near and far ends of the network. This leads to multiple delays in the transient response at the near and far ends of the network which can

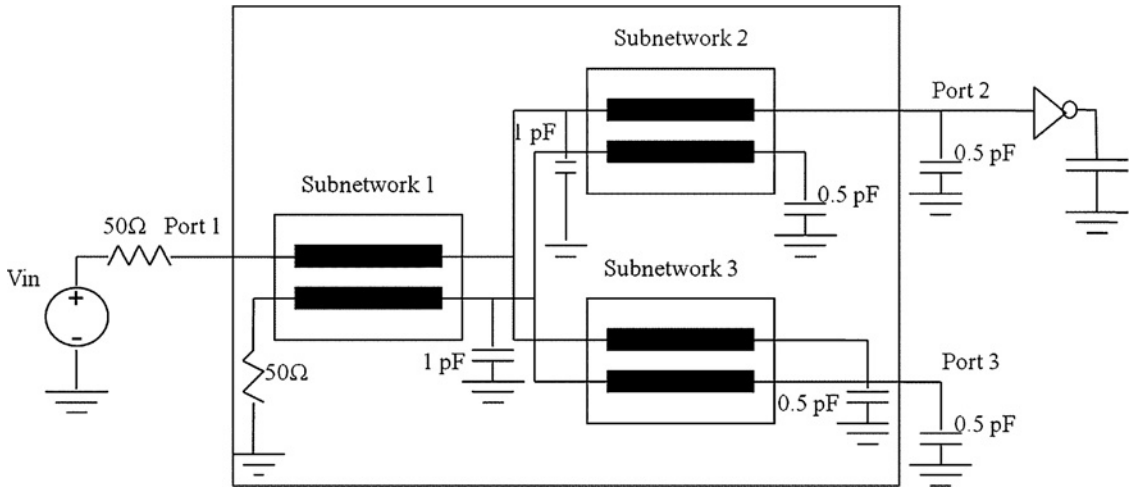

Fig. 9. Circuit of Example 3.

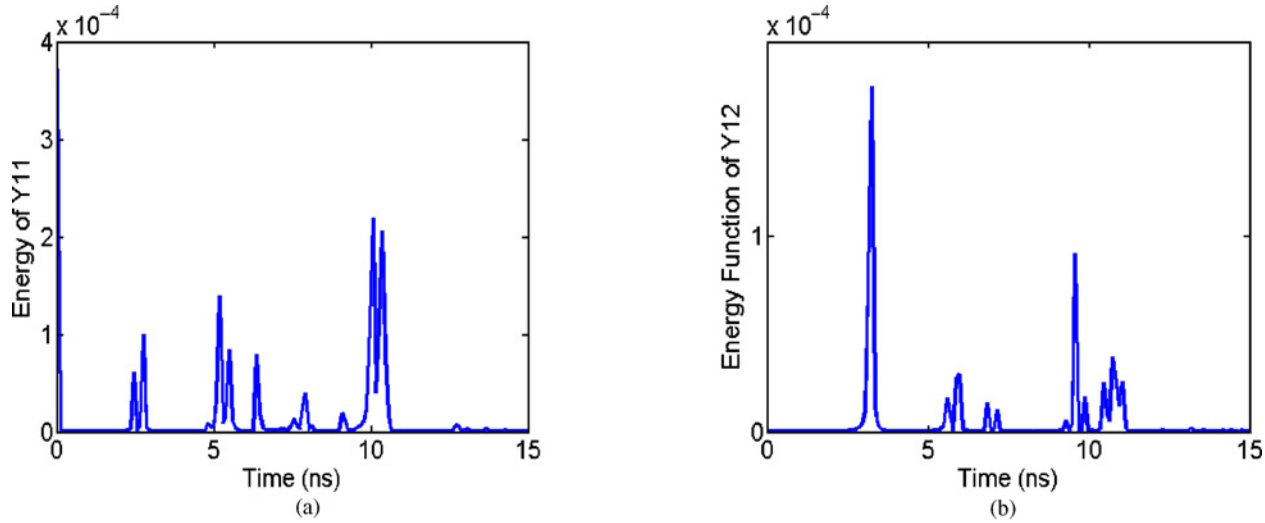

Fig. 10. Evaluating $\eta_{11}(\tau)$ and $\eta_{12}(\tau)$ of Example 3. (a) Energy of |Y11|($\eta_{11}(\tau)$). (b) Energy of |Y12|($\eta_{12}(\tau)$).

be analytically expressed as [12]

$$T_{11}^{(m)} = 2m * T_0$$
$$T_{12}^{(m)} = (2m-1) * T_0 \qquad m = \{1, 2...\} \tag{17}$$

where $T_{11}^{(m)}, T_{12}^{(m)}$ represent the delays of $Y_{11}^{(m)}, Y_{12}^{(m)}$, respectively, and m is an integer. To validate the accuracy of the proposed delay extraction methodology, the network is characterized by its tabulated $\boldsymbol{Y}$ parameters data over a bandwidth of 0–3.5 GHz. Using (5) and (6), the time-frequency transforms of $F_{ij}(\omega, \tau)$ and the energy spectrums of $\eta_{ij}(\tau)$ for all entries of the Y-parameter matrix are evaluated. The energy functions of $\eta_{11}(\tau)$ and $\eta_{12}(\tau)$ are shown in Fig. 7. Next, using (9) and (10) where $\varepsilon = 1e-5$, the delay peaks are identified as shown in Table III. It is observed from Table III that the observed delays (T_k) show excellent agreement with the theoretical delay values of (17).

To obtain the attenuation loss responses in terms of sampled data, the (ω, τ) plane of $F_{ij}(\omega, \tau)$ is divided into Ω_m regions using (11) and (12), where $\delta = 1e-6$. The partitioning points for $Y_{11}(s)$ and $Y_{12}(s)$ are shown in Table IV. Once $\tilde{Y}_{ij}^{(m)}(s)$ are evaluated using the integral of (8), the associated attenuation losses $H_{ij}^{(m)}(s)$ are obtained using the Hilbert transform on $\tilde{Y}_{ij}^{(m)}(s)$ using (15) and (16). For a trapezoidal input pulse of rise time 0.1 ns and pulse width of 20 ns, the transient port responses obtained using the proposed algorithm are shown in Fig. 8. In addition, the proposed algorithm is compared with the HSPICE W-element model. It is observed that the proposed model gives good agreement with HSPICE's W-element and is similar to those reported in [9].

TABLE IV
TIME AXIS PARTITIONING OF (ω, τ) PLANE OF EXAMPLE 2

Ω_m Regions	Y_{11}	Y_{12}
Ω_1	$0 \le \tau \le 8$ ns	$0 \le \tau \le 16$ ns
Ω_2	$8 \le \tau \le 24$ ns	$16 \le \tau \le 32$ ns
Ω_3	$24 \le \tau \le 40$ ns	$32 \le \tau \le 48$ ns
Ω_4	$40 \le \tau \le 50$ ns	–

Example 3: A three-port example is considered as shown in Fig. 9. The linear network consists of three subnetworks,

TABLE V
DELAY IDENTIFICATION FOR EXAMPLE 3 USING TIME-FREQUENCY ANALYSIS

Identified Delays (ns)	Y_{11}	Y_{12}
T_1	2.44	3.22
T_2	2.73	5.57
T_3	4.79	5.96
T_4	5.18	6.84
T_5	5.47	7.13
T_6	6.35	9.28
T_7	7.52	9.57
T_8	7.91	9.86
T_9	9.08	10.45
T_{10}	10.06	10.74
T_{11}	10.35	11.04

TABLE VI
TIME AXIS PARTITIONING OF (ω, τ) PLANE OF EXAMPLE 3

Ω_m Regions	Y_{11}	Y_{12}
Ω_1	$0 \le \tau \le 1.25$ ns	$0 \le \tau \le 4.39$ ns
Ω_2	1.25 ns $\le \tau \le$ 3.70 ns	4.39 ns $\le \tau \le$ 6.55 ns
Ω_3	3.70 ns $\le \tau \le$ 6.06 ns	6.55 $\le \tau \le$ 7.72 ns
Ω_4	6.06 ns $\le \tau \le$ 7.00 ns	7.72 $\le \tau \le$ 10.25 ns
Ω_5	7.00 ns $\le \tau \le$ 8.50 ns	10.25 ns $\le \tau \le$ 11.00 ns
Ω_6	8.50 ns $\le \tau \le$ 11.00 ns	–

each consisting of two coupled transmission lines. The p.u.l. parameters of the subnetwork 1 are

$$\boldsymbol{R} = \begin{bmatrix} 0.252 & 0 \\ 0 & 0.252 \end{bmatrix} \Omega/\text{cm}$$
$$\boldsymbol{L} = \begin{bmatrix} 3.36 & 0.865 \\ 0.865 & 3.36 \end{bmatrix} \text{nH/cm}$$
$$\boldsymbol{C} = \begin{bmatrix} 1.29 & -0.197 \\ -0.197 & 1.29 \end{bmatrix} \text{pF/cm}$$
$$\boldsymbol{G} = 0 \text{ mho/cm}$$

and that of subnetworks 2 and 3 are

$$\boldsymbol{R} = \begin{bmatrix} 0.34 & 0 \\ 0 & 0.34 \end{bmatrix} \Omega/\text{cm}$$
$$\boldsymbol{L} = \begin{bmatrix} 4.76 & 1.1 \\ 1.1 & 4.76 \end{bmatrix} \text{nH/cm}$$
$$\boldsymbol{C} = \begin{bmatrix} 2 & -0.58 \\ -0.58 & 2 \end{bmatrix} \text{pF/cm}$$
$$\boldsymbol{G} = 0 \text{ mho/cm}.$$

The transmission line length of each subnetwork is set to 20 cm and is terminated with a nonlinear inverter. The network is characterized by its terminal responses ($\boldsymbol{Y}$-parameters) as tabulated data over a bandwidth of 0–7 GHz, generated using HSPICE. Next, (5) and (6) are used to obtain the time-frequency transforms of $F_{ij}(\omega, \tau)$ and the energy spectrums of $\eta_{ij}(\tau)$ for all the port-to-port $\boldsymbol{Y}$-parameters are evaluated. Fig. 10 illustrates the energy of $\eta_{11}(\tau)$ and $\eta_{12}(\tau)$, where the delays of the system are identified as the peaks of the functions using (9) and (10) and $\varepsilon = 1e-5$, as shown in Table V.

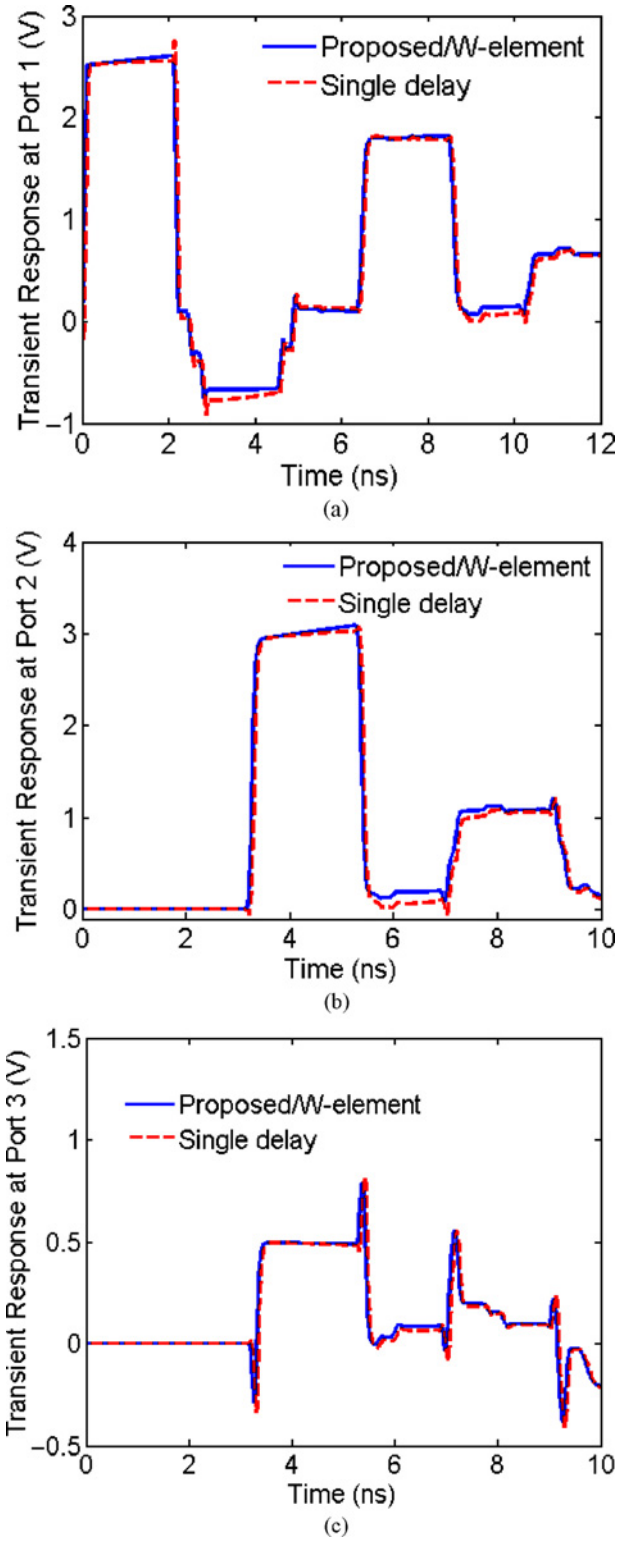

Fig. 11. Transient response of Example 3 using proposed algorithm and single delay method. (a) Response of Port 1. (b) Response of Port 2. (c) Response of Port 3.

To obtain the attenuation loss responses in terms of sampled data, the (ω, τ) plane of $F_{ij}(\omega, \tau)$ is divided into Ω_m regions using (11) and (12), where $\delta = 1e-6$. The partitioning points for $Y_{11}(s)$ and $Y_{12}(s)$ are shown in Table VI. Once $\tilde{Y}_{ij}^{(m)}(s)$ are evaluated using the integral of (8), the associated attenuation losses $H_{ij}^{(m)}(s)$ are obtained using the Hilbert transform on

$\tilde{Y}_{ij}^{(m)}(s)$ using (15) and (16). For a trapezoidal input pulse of rise time 0.05 ns and pulse width of 2 ns, the transient port responses obtained using the proposed algorithm are shown in Fig. 11. In addition, the proposed algorithm is compared with the single delay model based on numerical convolution [23] and the HSPICE W-element model. It is observed that the proposed model gives good agreement with HSPICE's W-element, while the single delay extraction model leads to different responses due to the non-negligible phase contribution of the multiple delays.

V. Conclusion

In this paper, a novel approach toward multiple delay extraction within a numerical convolution scheme was proposed for modeling distributed networks characterized by band limited frequency responses. The proposed algorithm uses time-frequency analysis to extract all propagation delays of a distributed network and to evaluate the associated attenuation losses in a piecewise manner, and implements IFFT to efficiently convert the frequency response into a sum of delayed time domain responses. Numerical convolution of the delay-causal response with any input provides accurate transient responses without the need for iterative curve fitting of the band limited data. The algorithm is tested for various multiport transmission line networks and was found to provide more accurate results compared to existing single delay extraction models based on numerical convolution techniques.

References

[1] W. T. Beyene and J. E. Schutt-Aine, "Accurate frequency-domain modeling and simulation of high-speed packaging interconnects," *IEEE Trans. Microw. Theory Tech.*, vol. 45, no. 10, pp. 1941–1947, Oct. 1997.

[2] W. T. Beyene and J. E. Schutt-Aine, "Efficient transient simulation of high-speed interconnects characterized by sampled data," *IEEE Trans. Compon. Packag. Manuf. Technol. Part B*, vol. 21, no. 1, pp. 105–114, Feb. 1998.

[3] M. Elzinga, K. L. Virga, L. Zhao, and J. L. Prince, "Pole-residue formulation for transient simulation of high-frequency interconnects using householder LS curve-fitting techniques," *IEEE Trans. Adv. Packag.*, vol. 23, no. 2, pp. 142–147, May 2000.

[4] M. Elzinga, K. L. Virga, L. Zhao, and J. L. Prince, "Improved global rational approximation macro-modeling algorithm for networks characterized by frequency sampled data," *IEEE Trans. Microw. Theory Tech.*, vol. 48, no. 9, pp. 1461–1468, Sep. 2000.

[5] B. Gustavsen and A. Semlyen, "Rational approximation of frequency domain responses by vector fitting," *IEEE Trans. Power Delivery*, vol. 14, no. 3, pp. 1052–1061, Jul. 1999.

[6] D. Saraswat, R. Achar, and M. Nakhla, "A fast algorithm and practical considerations for passive macromodeling of measured/simulated data," *IEEE Trans. Compon. Packag. Manuf. Technol. Part B*, vol. 27, no. 1, pp. 57–70, Feb. 2004.

[7] M. Tang and J. F. Mao, "Finite-difference analysis of interconnects with frequency-dependent parameters based on equivalent circuit models," *IEEE Trans. Adv. Packag.*, vol. 33, no. 2, pp. 457–467, May 2010.

[8] A. Charest, D. Saraswat, M. Nakhla, R. Achar, and N. Soveiko, "Compact macromodeling of high-speed circuits via delayed rational functions," *IEEE Microw. Wirel. Compon. Lett.*, vol. 17, no. 12, pp. 828–830, Dec. 2007.

[9] A. Charest, M. S. Nakhla, R. Achar, D. Saraswat, N. Soveiko, and I. Erdin, "Time domain delay extraction-based macromodeling algorithm for long-delay networks," *IEEE Trans. Adv. Packag.*, vol. 33, no. 1, pp. 219–235, Feb. 2010.

[10] S. Grivet-Talocia, "Delay-based macromodels for long interconnects via time-frequency decompositions," in *Proc. IEEE Electr. Performance Electron. Packag.*, Oct. 2006, pp. 199–202.

[11] A. Chinea, P. Triverio, and S. Grivet-Talocia, "Compact macromodeling of electrically long interconnects via time-frequency decompositions," in *Proc. IEEE Electr. Performance Electron. Packag.*, Oct. 2008, pp. 199–202.

[12] A. Chinea, P. Triverio, and S. Grivet-Talocia, "Delay-based macromodeling of long interconnects from frequency-domain terminal responses," *IEEE Trans. Adv. Packag.*, vol. 33, no. 1, pp. 246–256, Feb. 2010.

[13] P. Triverio, S. Grivet-Talocia, and A. Chinea, "Black-box identification of delay-based macromodels from measured terminal responses," in *Proc. 13th IEEE Signal Propag. Interconnects Workshop*, May 2009, pp. 1–4.

[14] P. Triverio, S. Grivet-Talocia, and A. Chinea, "Identification of highly efficient delay-rational macromodels of long interconnects from tabulated frequency data," *IEEE Trans. Microw. Theory Tech.*, vol. 58, no. 3, pp. 566–577, Mar. 2010.

[15] B. Zhong, D. Hu, T. Fu, S. L. Dvorak, and J. L. Prince, "A study of hybrid phase-pole macromodel for transient simulation of complex interconnects structures," *IEEE Trans. Comput.-Aided Des. Integr. Circuits Syst.*, vol. 24, no. 2, pp. 1250–1261, Aug. 2005.

[16] C. P. Coelho, J. R. Phillips, and L. M. Silveira, "A convex programming approach for generating guaranteed passive approximations to tabulated frequency data," *IEEE Trans. Comput.-Aided Des. Integr. Circuits Syst.*, vol. 48, no. 9, pp. 293–301, Sep. 2004.

[17] G. Antonini, "SPICE equivalent circuits of frequency-domain responses," *IEEE Trans. Eletromag. Compatibility*, vol. 45, no. 8, pp. 502–512, Aug. 2003.

[18] S. Min and M. Swaminathan, "Construction of broadband passive macromodels from frequency data for simulation of distributed interconnect networks," *IEEE Trans. Eletromag. Compatibility*, vol. 46, no. 4, pp. 544–558, Nov. 2004.

[19] A. R. Djordevic and T. K. Sarkar, "Transient analysis of electromagnetic systems with multiple lumped nonlinear loads," *IEEE Trans. Antennas Propag.*, vol. 33, no. 5, pp. 533–539, May 1985.

[20] D. Winklestein, M. B. Steer, and R. Pomerleau, "Simulation of arbitrary transmission line networks with nonlinear terminations," *IEEE Trans. Circuits Syst.*, vol. 38, no. 4, pp. 418–422, Apr. 1991.

[21] L. P. Vakanas, A. C. Cangellaris, and O. A. Palusinski, "Scattering parameter-based simulation of transients in lossy nonlinearly terminated packaging interconnections," *IEEE Trans. Compon. Packag. Manuf. Technol. B*, vol. 17, no. 4, pp. 472–479, Nov. 1994.

[22] M. S. Basel, M. B. Steer, and P. D. Franzon, "Simulation of high speed interconnects using a convolution-based hierarchical simulator," *IEEE Trans. Compon. Packag. Manuf. Technol. B*, vol. 18, no. 1, pp. 74–82, Feb. 1995.

[23] S. N. Lalgudi, E. Engin, G. Casinovi, and M. Swaminathan, "Accurate transient simulation of interconnect characterized by band-limited data with propagation delay enforcement in a modified nodal analysis framework," *IEEE Trans. Eletromag. Compatibility*, vol. 50, no. 3, pp. 715–729, Aug. 2008.

[24] R. Mandrekar and M. Swaminathan, "Causality enforcement in transient simulation of passive networks through delay extraction," in *Proc. 9th IEEE Workshop Signal Propag. Interconnects*, May 2005, pp. 25–28.

[25] R. Mandrekar, K. Srinivasan, E. Engin, and M. Swaminathan, "Causal transient simulation of passive networks with fast convolution," in *Proc. 10th IEEE Workshop Signal Propag. Interconnects*, May 2006, pp. 61–64.

[26] F. H. Branin, Jr., "Transient analysis of lossless transmission lines," *Proc. IEEE*, vol. 55, no. 11, pp. 2012–2013, Nov. 1967.

[27] S. Grivet-Talocia, H. M. Huang, A. E. Ruehli, F. Canavero, and I. M. Elfadel, "Transient analysis of lossy transmission lines: An efficient approach based on the method of characteristics," *IEEE Trans. Adv. Packag.*, vol. 27, no. 1, pp. 45–56, Feb. 2004.

[28] I. M. Elfadel, H.-M. Huang, A. E. Ruehli, A. Dounavis, and M. S. Nakhla, "A comparative study of two transient analysis algorithms for lossy transmission lines with frequency-dependent data," *IEEE Trans. Adv. Packag.*, vol. 25, no. 5, pp. 143–153, May 2002.

[29] A. Dounavis and V. Pothiwala, "Passive closed-form transmission line macromodel using method of characteristics," *IEEE Trans. Adv. Packag.*, vol. 31, no. 1, pp. 190–202, Feb. 2008.

[30] A. Dounavis, V. Pothiwala, and A. Beygi, "Passive macromodeling of lossy multiconductor transmission lines based on the method of characteristics," *IEEE Trans. Adv. Packag.*, vol. 32, no. 1, pp. 184–198, Feb. 2009.

[31] S. Lin and E. S. Kuh, "Transient simulation of lossy interconnects based on a recursive convolution formulation," *IEEE Trans. Circuits Syst. I: Fundam. Theory Appl.*, vol. 39, no. 11, pp. 879–892, Nov. 1992.
[32] F. M. Tesche, "On the use of the Hilbert transform for processing measured CW data," *IEEE Trans. Eletromag. Compatibility*, vol. 34, no. 3, pp. 259–266, Aug. 1992.
[33] S. L. Hahn, *Hilbert Transforms in Signal Processing*, 2nd ed. Norwood, MA: Artech House, 1996.
[34] A. Oppenheim and R. Schafer, *Discrete-Time Signal Processing*, 2nd ed. Englewood Cliffs, NJ: Prentice-Hall, 1999.
[35] S. K. Mitra, *Digital Signal Processing A Computer Based Approach*, 3rd ed. New York, McGraw-Hill, 2006.
[36] D. Gabor, "Theory of communications," *J. Inst. Electr. Eng.*, vol. 93, no. 3, pp. 429–457, 1946.
[37] J. Yao and P. Krolak, "The generalized Gabor transform," *IEEE Trans. Image Process.*, vol. 4, no. 7, pp. 978–988, Jul. 1995.
[38] A. I. Zayed, *Handbook of Function and Generalized Function Transformation*. New York: CRC Press, 1996.
[39] L. Mansinha, R. Stockwell, and R. Lowe, "Local S-spectrum analysis of 1-D and 2-D data," *Phys. Earth Planetary Interiors*, vol. 103, nos. 3–4, pp. 329–336, Nov. 1997.
[40] R. Stockwell, L. Mansinha, and R. Lowe, "Localization of the complex spectrum: The S transform," *IEEE Trans. Signal Process.*, vol. 44, no. 4, pp. 998–1001, Apr. 1996.
[41] *HSPICE U-2008.09-RA*, Synopsys, Mountain View, CA, Sep. 2008, pp. 4.28–4.44.
[42] *HSPICE Signal Integrity User Guide*, Synopsys, Mountain View, CA, Sep. 2005, pp. 61–113.
[43] R. Achar and M. Nakhla, "Simulation of high-speed interconnects," *Proc. IEEE*, vol. 89, no. 5, pp. 693–728, May 2001.
[44] S. Y. Kim, N. Gopal, and L. T. Pillage, "Time-domain macromodels for VLSI," *IEEE Trans. Comput.-Aided Design Integr. Circuits Syst.*, vol. 13, no. 10, pp. 1257–1270, Oct. 1994.

Sourajeet Roy received the B.Tech. degree in electrical engineering from Sikkim Manipal University, Gangtok, India, in 2006, and the M.E.Sc. degree from the University of Western Ontario, London, ON, Canada, in 2009. He is currently working toward the Ph.D. degree from the Department of Electrical and Computer Engineering, University of Western Ontario.

His current research interests include numerical algorithms for efficient transient simulation of high-speed packages.

Mr. Roy was the recipient of the Vice-Chancellors Gold Medal for Academic Excellence at the undergraduate level.

Anestis Dounavis (S'00–M'03) received the B.Eng. degree in electrical engineering from McGill University, Montreal, QC, Canada, in 1995, and the M.S. and Ph.D. degrees in electrical engineering from Carleton University, Ottawa, ON, Canada, in 2000 and 2004, respectively.

He is currently an Associate Professor with the Department of Computer and Electrical Engineering, University of Western Ontario, London, ON. His current research interests include electronic design automation, simulation of high-speed and microwave networks, signal integrity, and numerical algorithms.

Dr. Dounavis was the recipient of the Ottawa Center for Research and Innovation Futures Award—Student Researcher of the Year in 2004 and the INTEL Best Student Paper Award at the Electrical Performance of Electronic Packaging Conference in 2003. He received the Carleton University Medal for Outstanding Graduate Work at the M.S. and Ph.D. levels, in 2000 and 2004, respectively.